# Nonlocal pseudopotentials in complex bandstructure and photoemission calculations

A. Bödicker and W. Schattke
Institut für Theoretische Physik, Leibnizstr. 15, D-24118 Kiel, Germany



Basing on a recently proposed localization procedure, a nonlocal pseudopotential scheme is derived to calculate potential coefficients $V_{\vec{G}\vec{G}'}(\vec{k})$ which can be decomposed into terms, each being quadratic in $\vec{k}$ and multiplied by a function of $(\vec{G}-\vec{G}')$, thus making them applicable to some important cases where local potential coefficients are required. Electronic structure calculations for semiconductors are in agreement with well known semiempirical local pseudopotential bandstructures, as shown for GaAs. Nevertheless, the potential may significantly deviate from the semiempirical results. In order to test wavefunctions and transition probabilities we prove the success of the procedure in a more troublesome case, i. e. applying it to a transition metal compound as the experimentally well investigated layered crystal $TiSe_2$ which up to now was not treated with a pseudopotential. Photoemission spectra within the one–step model are presented using Pendry's method of complex bandstructure calculation. The latter formalism had to be slightly generalized for the quasi–local properties of the potential. The agreement of the spectra with experimental data shows this method to be a reliable and practical tool to use nonlocal pseudopotentials for conduction band wave functions of electron spectroscopies.

71.15.Hx, 79.60.Jv

## I. INTRODUCTION

The widely used empirical local pseudopotentials [1–11], as e. g. introduced by Cohen and Bergstresser [12], are attractive because of their simplicity, relying only on a few elements derived from fitting to optical data. The property of being local allows for a reduction of computational efforts. This is not relevant in standard bandstructure determinations but it is helpful in tasks which need a bandstructure computation as a single and often repeated step [13] and crucially arises in the computation of complex bandstructures as needed e. g. in the calculation of the photoemission spectra [9] or of the spectra of elastically diffracted electrons at very low energies (VLEED) [6,8,11]. Especially, in the latter case the scattering states are conveniently obtained via Pendry's technique to solve the inverse problem for the complex bandstructure, which in its simplest form requires a local potential [14].

In view of these advantages two drawbacks prove to be cumbersome in actual applications, firstly the lack of an "ab–initio" base and secondly the problem of generating the potential coefficients. Apart from the tabulated zincblende potentials, suitable coefficients have to be found by an unsatisfying trial and error procedure. Depending on the system under consideration, it may not converge at all.

In contrast to this situation, a well tested technique for the construction of ab–initio atomic pseudopotentials exists [15–17]. They principally depend on angular momentum in a nonlocal way which would prohibit an application to the above class of problems. However, recently a method was presented to convert these potentials to a local hamiltonian atomic potential [18]. It was intended to serve Monte–Carlo–Simulations. We could benefit from that development in constructing crystal potentials which after a simple generalization of Pendry's method are conveniently applied to electron spectroscopy. With a straightforward determination of the potential coefficients in a plane wave basis [19] we are able to generate a potential for layered dichalcogenides, hitherto not successfully treated in the pseudopotential scheme.

In this paper we report our applications of the novel pseudopotential of Bachelet et al. to GaAs for the reason of comparing it with the standard local potential, and to the layered crystal $TiSe_2$ for showing its success in treating complex systems. We shortly outline the conversion from a nonlocal to a quasi–local potential of the solid.

## II. METHOD OF CALCULATION

The matrix elements of the separable generalized norm–conserving pseudopotentials by Hamann [17] are calculated as

$$\langle \Phi_1 \mid V \mid \Phi_2 \rangle = \sum_{l=0}^{\infty} \sum_{m=-l}^{l} \int d\vec{r} \int d\vec{r}\,' \cdot$$
$$\cdot \Phi_1^*(\vec{r})\, Y_{lm}(\hat{r})\, V_l(r)\, \frac{\delta(r-r')}{r^2}\, Y_{lm}^*(\hat{r}')\, \Phi_2(\vec{r}\,') \qquad (1)$$

This potential is local in $r$ and nonlocal in $\theta$ and $\phi$. Replacing Eq. (1) Bachelet et al. introduced a local pseudopotential matrix [18]

$$\langle \Phi_1 \mid V \mid \Phi_2 \rangle = \int d\vec{r} \int d\vec{r}\,' \langle \Phi_1 \mid \vec{r}\,' \rangle\, \delta(\vec{r}-\vec{r}\,') \cdot$$
$$\cdot \left[ v(r) - \frac{1}{2}\, \nabla a(r) \nabla + b(r)\, \frac{\mathbf{L}^2}{2r^2} \right] \langle \vec{r} \mid \Phi_2 \rangle \qquad (2)$$

which reproduces the action of the nonlocal pseudopotentials with respect to the angular–momentum dependence. Outside the core, the radial functions $a(r)$ and $b(r)$ must vanish and $v(r)$ should asymptotically vanish as $-Z_v/r$ ($Z_v$ is the valence charge). The three unknown functions can be determined by requiring that the three lowest $l$ radial eigenfunctions $u_l(r)$ and eigenvalues $E_l$ of the radial Schrödinger equation are identical for both pseudopotentials. This restriction leads to the following system of three differential equations

$$\left[ a \frac{d^2}{dr^2} - (a+b)\, \frac{l(l+1)}{r^2} + \frac{da}{dr} \left( \frac{d}{dr} - \frac{1}{r} \right) - 2(v - V_l) \right] u_l = 0 \qquad (3)$$

with $V_l$ being the norm–conserving pseudopotential by Hamann [17]. Choosing the simple analytic form $a(r) = a_0 \exp(-(r/r_c)^k)$, $a_0 = 0.9$, $r_c = 1.0$ and $k = 2$, proposed in Ref. [18], Eq. (3) for $l = 0, 1$ is used to determine $b$ and $v$:

$$v = a\, \frac{u_0''}{2u_0} + a' \left[ \frac{u_0'}{2u_0} - \frac{1}{2r} \right] + V_0$$
$$b = -a + a\, \frac{r^2 u_l''}{l(l+1)u_l} + a'\, \frac{r^2 u_l' - r u_l}{l(l+1)u_l} - 2\, \frac{[v - V_l] r^2}{l(l+1)}$$

We adapted the atomic pseudopotential to the solid by calculating the atomic matrix elements $\langle \vec{k} + \vec{G} \mid V \mid \vec{k} + \vec{G}' \rangle = V_{\vec{G}\vec{G}'}(\vec{k})$ in a basis of plane waves with Bloch vector $\vec{k}$ and reciprocal lattice vector $\vec{G}$. For $\vec{G} \neq \vec{G}'$ one gets

$$V_{\vec{G}\vec{G}'}(\vec{k}) = v_{\Delta\vec{G}} + \vec{K} \cdot \vec{K}' a_{\Delta\vec{G}} + \vec{K}'^2 \left( u^{(1)}_{\Delta\vec{G}} - u^{(2)}_{\Delta\vec{G}} \right)$$
$$+ \left[ \vec{K}' \cdot \Delta\vec{G} \right]^2 \left( -u^{(1)}_{\Delta\vec{G}} + 3u^{(2)}_{\Delta\vec{G}} \right) / \Delta\vec{G}^2$$
$$+ \vec{K}' \cdot \Delta\vec{G}\, \left( -2u^{(2)}_{\Delta\vec{G}} \right) \qquad (4)$$

where $\left( a_G\ ,\ u^{(1)}_G\ ,\ u^{(2)}_G\ ,\ v_G \right)$ are the threedimensional Fourier transforms of $\frac{1}{2}\Big( a(r)\ ,\ b(r)\ ,\ b(r)\, r \cos\theta/(Gr^2)\ ,$

$2v(r)\Big)$ with polar angle $\theta$ measured in a coordinate system with $\vec{G}$ being parallel to the $z$–axis, $\vec{K}^{(\prime)} = \vec{k} + \vec{G}^{(\prime)}$, and $\Delta\vec{G} = \vec{G}' - \vec{G}$. Because of rotational invariance the various coefficients depend only on the absolute value of $\vec{G}$. For $\vec{G} = \vec{G}'$, the formula simplifies to:

$$V_{\vec{G}\vec{G}} = (\vec{k} + \vec{G})^2 \left( a_0 + \frac{2}{3}\, u_0^{(1)} \right) + \mathrm{E_{shift}} \qquad (5)$$

$\mathrm{E_{shift}}$ pins the valence band maximum to the energy zero. These plane wave matrix elements previously have been used to accelerate the Car–Parinello iteration scheme [19].

## III. APPLICATION TO GAAS

Once the atomic potentials have been determined, it is straightforward to solve for the energy band spectrum, using the following elements of the Hamiltonian matrix

$$H_{\vec{G}\vec{G}'}(\vec{k}) = \frac{1}{2}\, (\vec{k} + \vec{G})^2\, \delta_{\vec{G}\vec{G}'} + S\, V_{\vec{G}\vec{G}'}(\vec{k}) \qquad (6)$$

where $V_{\vec{G}\vec{G}'}(\vec{k})$ now comprises the sum over the constituting atomic potentials, Eqs. (4) and (6). The strength $S$ of the potential is introduced as a parameter, the only one of this theory. It affects the overlap between the atomic electronic densities. Having calculated pseudopotential coefficients for the atoms, the overlap usually arises as being too small. Increasing the overlap is achieved by reducing the strength of the potential. The rearrangement of the electronic densities of free atoms to the electronic density in a crystal could be principally obtained by self-consistency loops. In a short cut, we estimated the parameter $S$ a posteriori. For Galliumarsenide, $S = 0.719$ gives the best agreement with former bandstructure calculations [12,20,21]. Note that this is opposite to the behaviour of atomic orbitals of an atomic all–electron calculation which usually contract upon being transferred to the solid. In a tight–binding calculation the overlap integrals determined e. g. with the widely used Clementi–Roetti data [22] prove to overestimate the interaction range, because the electronic environment of the crystal compresses the orbitals [9]. Here, in the pseudopotential approach, the orbitals expand. This seems to be the consequence of the calculational method. Using only one parameter represents a remarkable progress compared with the empirical pseudopotential methods, where all local coefficients had to be fitted to optical data [12] and where nonlocal correction terms were added to the local potentials [20,21].

Tables I and II list the pseudopotential coefficients for Arsenic and for Gallium. The energy shift $v_0 = \mathrm{E_{shift}}$ is not displayed, because it depends on the number of plane waves used and on the cut–off radius for the potential parameters. The minimum cut–off radius of $\sqrt{24}$ to get an adequate (valence) bandstructure becomes larger than $\sqrt{11}$ of the empirical pseudopotential calculations [12] because the number of coefficients of a Fourier expansion usually exceeds the number obtained by minimizing a set of fit parameters. Extending the cut–off radius does not change the bandstructure up to 30 eV appreciably.

An interesting simplification arises from the restriction to the bare local part of our potential, i. e. to the first term in Eq. (4), leading to minor deviations in the conduction bandstructure only. Table III shows the converted local part of the pseudopotential coefficients of this paper to be directly compared with those of Ref. [12].

Fig. 1 shows the quasi–local pseudopotential bandstructure (solid lines) in comparison with the semiempirical bandstructure by Cohen and Bergstresser [12] (dashed lines). We have used 137 plane waves in both calculations. Increasing the number of plane waves does not change the bands in the displayed energy region. The comparison of the two bandstructures obtained from differently determined pseudopotentials shows good agreement below the Fermi level. The optical gap of 1.5 eV is achieved in both calculations. Comparing the conduction bandstructures, the differences are no more negligible. This and differing wavefunctions will influence matrix elements and should lead to differences in theoretical electron spectroscopy.

## IV. APPLICATION TO TISE$_2$

As a prototype of a system withstanding a semiempirical pseudopotential approach, we have chosen a compound from the class of layered transition metal dichalcogenides, $TiSe_2$ [23]. The crystal structure may be described as a stack of identical layers, loosely bound to each other across a van–der–Waals gap. Each layer consists of a sheet of titanium atoms, sandwiched by two sheets of selenium atoms. The atomic pseudopotential coefficients of titanium and selenium have been determined using the calculation scheme outlined above restricting the angular momentum to $l = 2$ for the cation and to $l = 1$ for the anion.

In order to test the potential by its wavefunctions and matrix elements, photoemission spectra in $\Gamma$A–direction have been computed and compared with experimental data [24,25] and with former calculations [25].

The photoemission theory is based on the single particle one–step model outlined in Ref. [26]. Only the final states are determined from the quasi–local potential. The basis of the initial states is calculated within an empirical LCAO representation to account for the tight binding . The surface of the halfspace is properly taken into account by determining the layer and wave vector resolved

Green's function applying a highly convergent renormalization scheme [27]. The final state, a time inverse LEED state, is taken as a superposition of bulk wavefunctions

$$\Phi^*_{LEED} = \sum_n t_n \sum_{\vec{G}} \alpha^{(n)}_{\vec{G}}(\vec{k}_n) \exp\left[-i(\vec{k}_n + \vec{G})\cdot\vec{r}\right] \quad (7)$$

with coefficients $t_n$, being further decomposed into plane waves with coefficients $\alpha^{(n)}_{\vec{G}}$. Outside the crystal, the final state is written as a direct superposition of plane waves. The eigenfunctions of the Hamiltonian result from the calculation of the complex bandstructure considering an energy dependent imaginary part of the optical potential. In fact, we use two different descriptions of the Hamiltonian accounting for the special properties of initial and final states. The LCAO representation is a suitable tool to describe the rather localized valence electrons of the initial states. The conduction electrons representing the final states are free electron like because they are forbidden by the Pauli principle from entering the immediate neighbourhood of the ions already occupied by the valence electrons. The behavior of these nearly free electrons cannot be described by a localized (tight binding) basis but by a superposition of very few plane waves. In principle, the plane wave basis could be used also for the initial states. But localized states require a very large number of plane waves increasing the valence states' computational efforts which, however, should be kept low to leave space for the other parts of the photoemission code. Generally, the one–step model uses muffin–tin potentials being adequate for metallic systems but failing in the case of covalently bound solids. One common procedure to meet these difficulties is to employ eigenstates of different Hamiltonians for the initial localized and final extended states, and to work on the $\vec{p}\cdot\vec{A}$–scheme of the matrix elements [5,9,25,28].

To apply our quasi–local pseudopotential coefficients, the method proposed by Pendry [14] has to be generalized. For this purpose, the matrix equation

$$\sum_{\vec{G}'} \left[\left(\frac{1}{2}(\vec{k}+\vec{G})^2 - E\right)\delta_{\vec{G}\vec{G}'} + S\, V_{\vec{G}\vec{G}'}(\vec{k})\right]\alpha_{\vec{G}} = 0 \quad (8)$$

is rewritten by introducing an intermediate variable $\vec{\beta}$, with $\beta_{\vec{G}} = (k_\perp + G_\perp)\,\alpha_{\vec{G}}$,

$$\begin{array}{rcl} -\widehat{A}\,\vec{\beta} - (\widehat{B} - E\widehat{1})\,\vec{\alpha} &=& k_\perp\,\widehat{M}\,\vec{\beta} \\ \widehat{1}\,\vec{\beta} - \widehat{C}\,\vec{\alpha} &=& k_\perp\,\widehat{1}\,\vec{\alpha} \end{array}$$

where the matrices $\widehat{A}$, $\widehat{B}$, $\widehat{C}$ and $\widehat{M}$ are not depending on $k_\perp$, the surface perpendicular component of the wave vector $\vec{k}$. The matrix elements for $\Delta\vec{G} \neq 0$ are given by the following formulae:

$$\begin{aligned} A_{\vec{G}\vec{G}'} = {} & G_\perp\left(a_{\Delta\vec{G}} + \frac{1}{2}\,\delta_{\vec{G}'\vec{G}}\right) + G'_\perp\left(u^{(1)}_{\Delta\vec{G}} - u^{(2)}_{\Delta\vec{G}}\right) \\ & - G'_\perp(G'_\perp - G_\perp)^2\left(u^{(1)}_{\Delta\vec{G}} - 3u^{(2)}_{\Delta\vec{G}}\right)/\Delta\vec{G}^2 \\ & - 2(G'_\perp - G_\perp)\,u^{(2)}_{\Delta\vec{G}} \\ & - 2(G'_\perp - G_\perp)(\vec{k}_\parallel + \vec{G}_\parallel)\cdot(\vec{G}'_\parallel - \vec{G}_\parallel) \\ & \left(u^{(1)}_{\Delta\vec{G}} - 3u^{(2)}_{\Delta\vec{G}}\right)/\Delta\vec{G}^2 \end{aligned}$$

$$\begin{aligned} B_{\vec{G}\vec{G}'} = {} & (\vec{k}_\parallel + \vec{G}'_\parallel)\cdot(\vec{k}_\parallel + \vec{G}_\parallel)\left(a_{\Delta\vec{G}} + \frac{1}{2}\,\delta_{\vec{G}'\vec{G}}\right) \\ & + (\vec{k}_\parallel + \vec{G}'_\parallel)^2\left(u^{(1)}_{\Delta\vec{G}} - u^{(2)}_{\Delta\vec{G}}\right) \\ & - 2(\vec{k}_\parallel + \vec{G}'_\parallel)\cdot(\vec{G}'_\parallel - \vec{G}_\parallel)\,u^{(2)}_{\Delta\vec{G}} \\ & - [(\vec{k}_\parallel + \vec{G}'_\parallel)\cdot(\vec{G}'_\parallel - \vec{G}_\parallel)]^2\left(u^{(1)}_{\Delta\vec{G}} - 3u^{(2)}_{\Delta\vec{G}}\right)/\Delta\vec{G}^2 \end{aligned}$$

$$\begin{aligned} M_{\vec{G}\vec{G}'} = {} & a_{\Delta\vec{G}} + \frac{1}{2}\,\delta_{\vec{G}'\vec{G}} + u^{(1)}_{\Delta\vec{G}} - u^{(2)}_{\Delta\vec{G}} \\ & - (G'_\perp - G_\perp)^2\left(u^{(1)}_{\Delta\vec{G}} - 3u^{(2)}_{\Delta\vec{G}}\right)/\Delta\vec{G}^2 \end{aligned}$$

$$C_{\vec{G}\vec{G}'} = G'_\perp\,\delta_{\vec{G}\vec{G}'}$$

In case of $\Delta\vec{G} = 0$ these formulae are shorter and simpler.

This transformation of Eq. (8) is possible because of the special form of the quasi–local pseudopotential coefficients being at most quadratic in $k_\perp$. A generalized eigenvalue problem for the momentum eigenvalues $k_\perp$ has to be solved. In order to fix the parameters $S$ and $E_{shift}$ for the conduction bandstructure of $TiSe_2$, we calculated a target current spectrum (TCS) for $TiTe_2$ and compared it to experimental data. For the isoelectronic systems, $TiTe_2$ and $TiSe_2$, the same potential strength $S$ may be used. Values of $S = 0.2$ and $E_{shift} = -2.8$ eV lead to satisfactory agreement between theoretical and experimental first derivatives of the TCS data. Comparing the conduction bandstructures of $TiSe_2$ and $TiTe_2$ obtained with these parameters, the main difference is a simple shift of about 2.5 eV within the interesting energy region. Computing photoemission spectra of $TiSe_2$, it turns out that $E_{shift} = -1.8$ eV leads to even better agreement between calculated and experimental photoemission spectra. The strong reduction of the potential by the low value of $S$ is associated with the higher energy regime used here for the conduction states as opposed to the GaAs example where we focussed on the valence states. It is to be expected that an LDA treatment would screen the deep atomic Ti potentials by the mainly occupied Se–p states in the solid thus further reducing the potential felt by the unoccupied, especially the Ti–3d, states.

For the subsequent discussion of the photoemission, the valence part of the quasi–local pseudopotential bandstructure is of no importance. For completeness, we note some values of $S$ and $E_{shift}$ for that energy range. Taking the same $S$ as for the excited states, the resulting valence bands have an $E_{shift} = -13.5$ eV, i. e. the conduction bands have to be shifted by about 11.7 eV to higher energies to agree with the usual findings. However, in $\Gamma A$ direction the valence bandwidth of the more dispersive bands is too large and the nondispersive bands are seen at somewhat higher energies. For $S = 0.345$ and $E_{shift} = -13.1$ eV the shape of the valence bands look more reasonable, but from an initially almost satisfying position the conduction bands now shift down by $-E_{shift}$. For higher $S$ all bands flatten in $\Gamma A$ direction losing their similarity with the known bandstructure. The Se dominated bands mostly cover the valence regime whereas the Ti states dominate in the conduction bands. The atomic pseudopotential seems to be more reliable for Se than for Ti. As in the case of reducing the potential strength $S$ to much lower values because of the deep potential, here again this potential is responsible for the necessary high relative shift of the conduction bands to reach a reasonable position. This strong energy dependence of the parameters $S$ and $E_{shift}$ would require a kind of scissor operator if applied to photoemission. However, in view of our numerical program for the one–step model, we rely here on the LCAO representation of the valence bands which hitherto proved to reflect very accurately the actual positions of the valence bands.

Fig. 2 shows the computed photoemission spectra in $\Gamma A$–direction. Because there appears almost no valence band crossing along the $\Gamma A$–direction, the photoemission maxima can easily be assigned. Both peaks at the binding energy of -3 eV and near the Fermi level arise from the nearly nondispersive valence bands and are derived from inplane bonding orbitals whereas the maximum dispersing from -0.8 eV to -3 eV is derived from bonds perpendicular to the surface. In Ref. [29] a discussion of matrix elements can be found in terms of final states which are obtained from muffin–tin potentials. As the initial states used in those calculations are identical with ours, the difference has to be attributed solely to the complex bandstructure of the final states. Fig. 3 shows the complex bandstructure for the quasi–local pseudopotential in comparison with that of damped plane waves. In view of the muffin–tin complex bandstructure plotted in Ref. [29], our pseudopotential result is more related to the plane wave case than the muffin–tin result, though there are qualitative differences as the band splitting and bending. Especially, an enhanced fine structure appears in the imaginary part of $k_\perp$, which is important for the coupling of the bulk states to the vacuum. This similarity to the plane wave case is expected to become apparent in the photocurrent, too. The photocurrent with damped plane waves as final states displays only both dispersive bands, the remaining two nondispersive ones being connected with a high density of states are completely suppressed. Therefore plane wave features arising in the pseudopotential decrease the importance of the density of states in the photocurrent different from the muffin–tin case. A convincing agreement with experimental data of Anderson et al. [24] plotted in Fig. 2 can be stated. The variation of the relative intensities of photoemission peaks with photon energy and the relative intensities themselves are correctly reproduced by our numerical results. It should be added that the agreement with experiment seems to be better than that obtained with muffin–tin layer KKR final states in a former calculation of Pehlke et al. [25]. Especially, the dispersive structure is much more pronounced here. To our opinion the latter is a typical property of spectra calculated with pseudopotential as opposed to muffin–tin potential final states. The conduction band wavefunctions in the rather low vacuum ultraviolet photon regime seem to forbid the neglect of the interstitial potential in comparison with the strong spherical part.

As already stated in Ref. [30], the normal emission current from the surface parallel components of the light polarization vanishes for the free electron like damped plane waves as final states, i. e. only the identical representation of the initial states given mostly by the $p_z$–orbitals survives. As a result the dispersive structures will be enhanced. Hence the slight similarity of the pseudopotential bandstructure with the plane wave result explains our findings. From the convincing comparison with experiment one would clearly favour the pseudopotential. Additionally, this is supported by the following arguments. Firstly, it includes the interstitial potential. Secondly, a screening of the stronger muffin–tin potential seems to be physically necessary for the energetically high lying final states. Thirdly, because of its simplicity it is easy to calculate even off–normal photoemission spectra. The latter proved in the past to be difficult to obtain in the case when a muffin–tin potential for the final states is connected with an anisotropic potential for the initial states as forced by the anisotropic bindings of the layered crystals.

## V. CONCLUSIONS

In concluding, the quasi–local pseudopotential derived from an ab–initio nonlocal potential has proven its applicability to complex systems. It is constructed in a straightforward manner employing one adjustable parameter, the only a posteriori element of the scheme. Thus, this method should be suitable for the wide class of materials the actual sophisticated pseudopotentials are made for. Because of its simplicity it could be successfully used in a VLEED calculation for the determination of target current spectra. Additionally, in representing a nonspherical potential for the final states of photoemission, it is superior to the alternative use of standard muffin–tin potentials in covalent solids. It would be interesting to see whether this potential works also in the case of the bounded states of a surface system.

We would like to thank M. Boehme for making available to us TCS measurements prior to publication and S. Brodersen for test calculations on GaAs. This work was financially supported by the Bundesministerium für Bildung, Wissenschaft, Forschung und Technologie under contract no. 05 605 FKA.

---

[1] A. L. Wachs, T. Miller, T. C. Hsieh, A. P. Shapiro, and T.–C. Chiang, *Phys. Rev. B* **32**, 2326 (1985).

[2] G. P. Williams, F. Cerrina, G. J. Lapeyre, J. R. Anderson, R. J. Smith, and J. Hermanson, *Phys. Rev. B* **34**, 5548 (1986).

[3] D. Straub, L. Ley, and F. J. Himpsel, *Phys. Rev. B* **33**, 2607 (1986).

[4] R. D. Bringans, R. I. G. Uhrberg, and R. Z. Bachrach, *Phys. Rev. B* **34**, 2373 (1986).

[5] J. Olde, K.–M. Behrens, H.–P. Barnscheidt, R. Manzke, M. Skibowski, J. Henk, and W. Schattke, *Phys. Rev. B* **44**, 6312 (1991).

[6] V. N. Strocov, *Solid State Commun.* **78**, 845 (1991).

[7] N. Sano and A. Yoshii, *Phys. Rev. B* **45**, 4171 (1992).

[8] J.–V. Peetz, W. Schattke, H. Carstensen, R. Manzke, and M. Skibowski, *Phys. Rev. B* **46**, 10127 (1992).

[9] J. Henk, W. Schattke, H. Carstensen, R. Manzke, and M. Skibowski, *Phys. Rev. B* **47**, 2251 (1993).

[10] M. Reigrotzki, M. Stobbe, R. Redmer, and W. Schattke, *Phys. Rev. B* **52**, 1456 (1995).

[11] V. N. Strocov and H. I. Starnberg, *Phys. Rev. B* **52**, 8759 (1995).

[12] M. L. Cohen and T. K. Bergstresser, *Phys. Rev.* **141**, 789 (1966).

[13] M. C. Payne, M. P. Teter, D. C. Allan, T. A. Arias and J. D. Joannopoulos, *Rev. Mod. Phys.* **64**, 1045 (1992).

[14] J. B. Pendry, *J. Phys. C* **2**, 2273 (1969).

[15] D. R. Hamann, M. Schlüter, and C. Chiang, *Phys. Rev. Lett.* **43**, 1494 (1979).

[16] G. B. Bachelet, D. R. Hamann, and M. Schlüter, *Phys. Rev. B* **26**, 4199 (1982).

[17] D. R. Hamann, *Phys. Rev. B* **40**, 2980 (1989).

[18] G. B. Bachelet, D. M. Ceperley, and M. G. B. Chiocchetti, *Phys. Rev. Lett.* **62**, 2088 (1989).

[19] W.M.C. Foulkes and M. Schlüter, *Phys. Rev. B* **42**, 11505 (1990).

[20] J. R. Chelikowsky and M. L. Cohen, *Phys. Rev. B* **14**, 556 (1976).

[21] T. P. Humphreys and G. P. Srivastava, *phys. stat. sol. (b)* **112**, 581 (1982).

[22] E. Clementi and C. Roetti, *At. Data Nucl. Data Tables* **14**, 177 (1974).

[23] J. A. Wilson and A. D. Yoffe, *Adv. Phys.* **18**, 193 (1969).

[24] O. Anderson, R. Manzke, and M. Skibowski, *Phys. Rev. Lett.* **55**, 2188 (1985).

[25] E. Pehlke, W. Schattke, O. Anderson, R. Manzke, and M. Skibowski, *Phys. Rev. B* **41**, 2982 (1990).

[26] P. J. Feibelman and D. E. Eastman, *Phys. Rev. B* **10**, 4932 (1974).

[27] J. Henk and W. Schattke, *Comput. Phys. Commun.* **77**, 69 (1993).

[28] D. Samuelsen and W. Schattke, *Surf. Sci.* **327**, 379 (1995).

[29] E. Pehlke and W. Schattke, *J. Phys. C: Solid State Phys.* **20**, 4437 (1987).

[30] E. Pehlke and W. Schattke, *Solid State Commun.* **69**, 419 (1989).

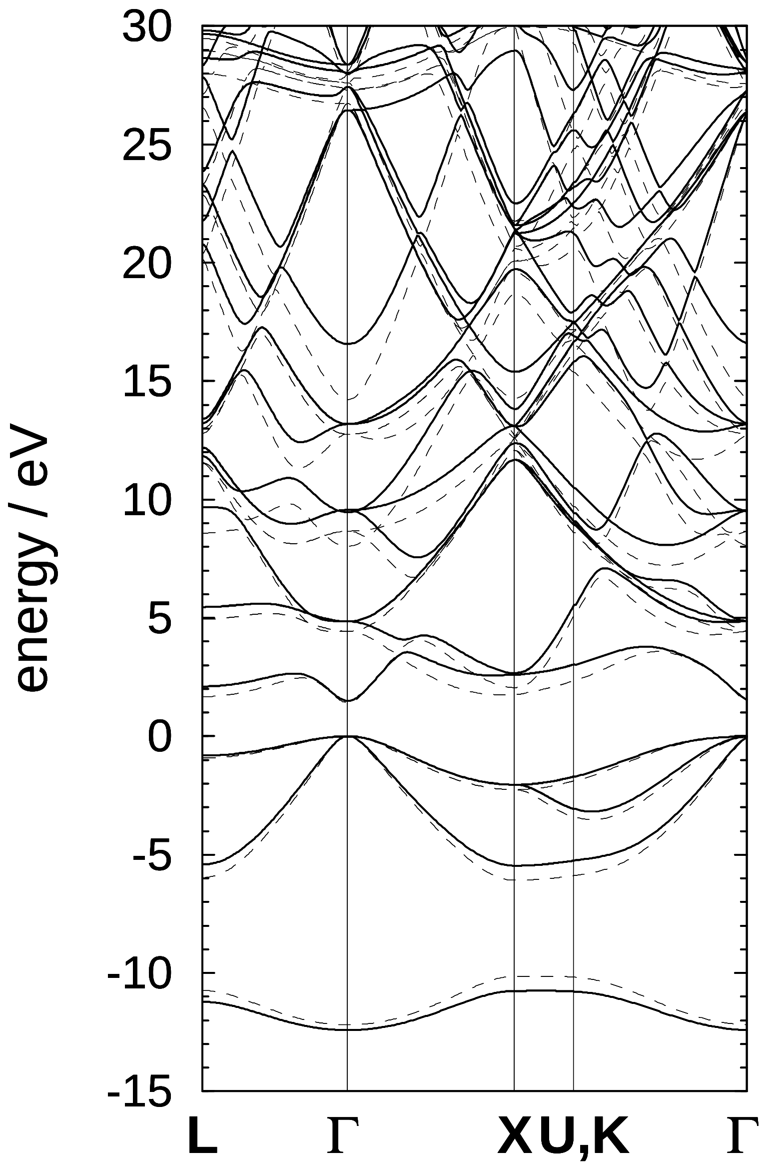


FIG. 1. Bandstructure of GaAs calculated with pseudopotential coefficients of this paper (solid lines) and from Ref. [12] (dashed lines).

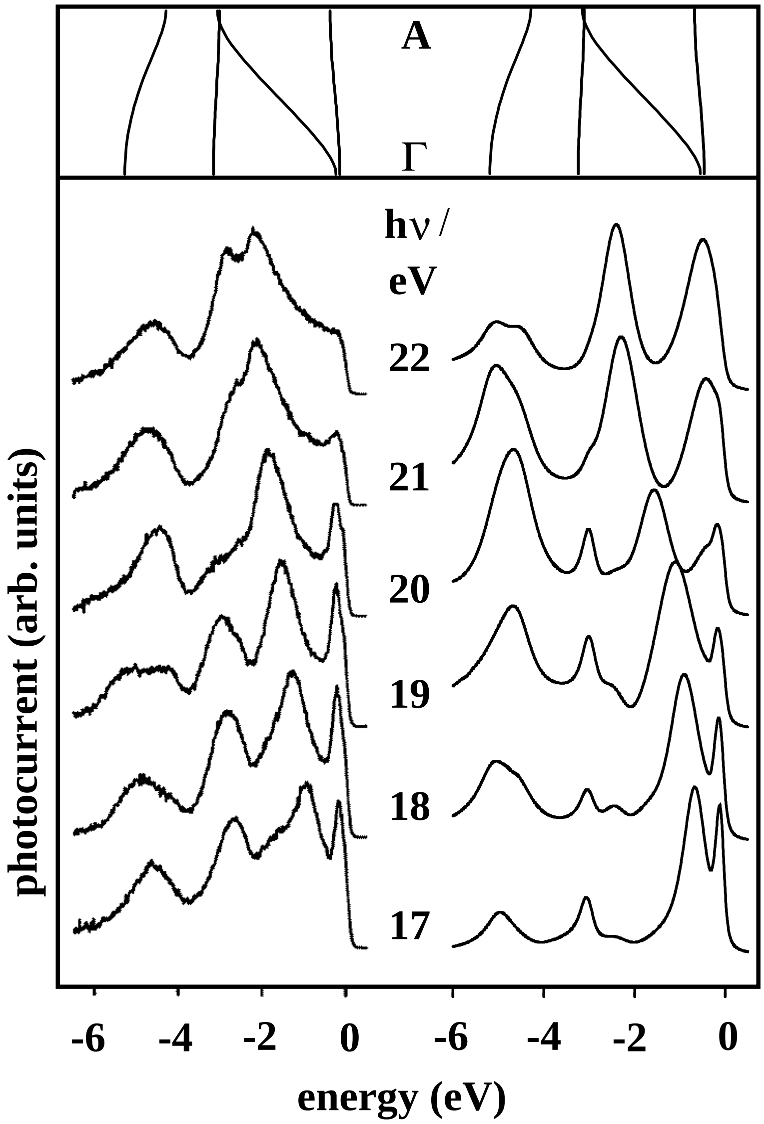


FIG. 2. Calculated (right side) and experimental (left side, taken from Ref. [24]) surface normal photoemission spectra for $TiSe_2$ . The plots of the photocurrent vs. binding energy are characterized by the value of the photon frequency. The upper panel shows the ΓA valence bandstructure being repeated for the binding energy scales of both sets of spectra.

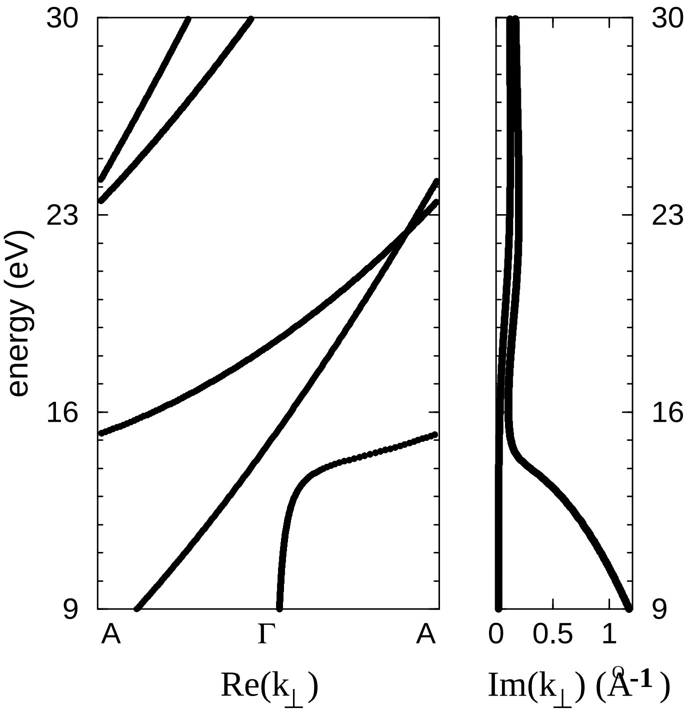


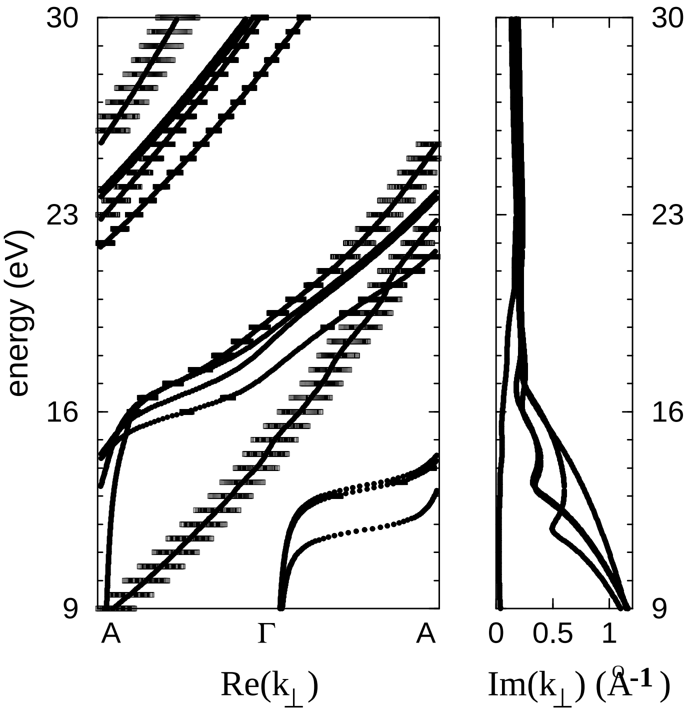


FIG. 3. The complex bandstructure of $TiSe_2$ for $\vec{k}_{\|} = 0$. In the left–hand panels the real part $\mathrm{Re}(k_\perp)$ is shown from bottom to top of the Brilloun zone. In the right–hand panels the imaginary part $\mathrm{Im}(k_\perp)$ is plotted. For the upper figure, damped plane waves have been used, whereas the lower part has been calculated with the quasi–local pseudopotentials. The length of the horizontal bars represents the transition probability, i. e. the squared modulus of the expansion coefficients $t_n$, see Eq. 7 in the photoemission computation.

TABLE I. Pseudopotential coefficients for Arsenic, units are $(2\pi/a)^2$ ($a$ lattice constant) for the first column, Hartree for the next column and Hartree$\cdot$(Bohr)$^2$ for the last three columns.

| $G^2$ | $v_G$ | $a_G$ | $u_G^{(1)}$ | $u_G^{(2)}$ |
|---|---|---|---|---|
| 0 | | -0.01644 | 0.00772 | 0.00000 |
| 3 | -0.11679 | -0.01269 | 0.00762 | 0.00303 |
| 4 | -0.06921 | -0.01164 | 0.00658 | 0.00279 |
| 8 | -0.00346 | -0.00823 | 0.00348 | 0.00203 |
| 11 | 0.01010 | -0.00635 | 0.00201 | 0.00159 |
| 12 | 0.01232 | -0.00582 | 0.00164 | 0.00147 |
| 16 | 0.01609 | -0.00412 | 0.00060 | 0.00108 |
| 19 | 0.01589 | -0.00318 | 0.00018 | 0.00086 |
| 20 | 0.01555 | -0.00292 | 0.00008 | 0.00080 |
| 24 | 0.01336 | -0.00206 | -0.00013 | 0.00061 |

TABLE II. Pseudopotential coefficients for Gallium, for units see Table I.

| $G^2$ | $v_G$ | $a_G$ | $u_G^{(1)}$ | $u_G^{(2)}$ |
|---|---|---|---|---|
| 0 | | -0.01644 | 0.00699 | 0.00000 |
| 3 | -0.05305 | -0.01269 | 0.00730 | 0.00284 |
| 4 | -0.02437 | -0.01164 | 0.00639 | 0.00264 |
| 8 | 0.01375 | -0.00823 | 0.00337 | 0.00195 |
| 11 | 0.02008 | -0.00635 | 0.00173 | 0.00152 |
| 12 | 0.02080 | -0.00582 | 0.00128 | 0.00140 |
| 16 | 0.02045 | -0.00412 | -0.00005 | 0.00097 |
| 19 | 0.01851 | -0.00318 | -0.00066 | 0.00072 |
| 20 | 0.01773 | -0.00292 | -0.00080 | 0.00065 |
| 24 | 0.01433 | -0.00206 | -0.00111 | 0.00042 |

TABLE III. Local pseudopotential coefficients in eV.

| | $V_3^S$ | $V_8^S$ | $V_{11}^S$ | $V_3^A$ | $V_4^A$ | $V_{11}^A$ |
|---|---|---|---|---|---|---|
| this paper | -3.32 | 0.20 | 0.59 | 1.25 | 0.88 | 0.19 |
| Ref. [12] | -3.13 | 0.14 | 0.82 | 0.95 | 0.68 | 0.14 |